Is there a linkage between the tropical cyclone activity in the southern Indian Ocean and the Antarctic Oscillation?

Rui Mao,[1] Dao-Yi Gong,[1] Jing Yang,[1] Zi-Yin Zhang,[2] Seong-Joong Kim,[3] and Hao-Zhe He [1,4]

[1] In this article, the relationship between the Antarctic Oscillation (AAO) and the tropical cyclone (TC) activity in the southern Indian Ocean (SIO) was examined. It was found that on the interannual time scale, the AAO is well linked with the TC activity in the SIO during TC season (December–March). The rank correlation coefficient between the AAO index and the TC frequency (TCF) in the SIO is 0.37, which is significant at the 95% confidence level. When the AAO is in a positive phase, TC passage in the northwestern coast of Australia (100E°–120°E and 10°S–30°S) increases by approximately 50%–100% from the climatology. The increase in the TC passage is primarily the result of more frequent TCs originating in this region due to enhanced water vapor convergence and ascending motions, which are caused by a cyclonic height anomaly over the western coast of Australia associated with the positive AAO phases. In addition, the AAO-height covariations, which are essential to the formation of the AAO-TC links in the SIO, were investigated through a historical climate simulation using the Community Climate System Model 4 from the Coupled Model Intercomparison Project Phase 5. The AAO-height links were well reproduced in the simulation. The similarity in the AAO-height links between the observation and the simulation supports the physical robustness of the AAO-TC links in the SIO.

1. Introduction

[2] Tropical cyclones (TCs) are a recurring phenomenon in the southern Indian Ocean (SIO) that most frequently occur in the period of November–April [*Ramsay et al.*, 2012]. The TC activities pose a significant threat to the communities that lie in their paths, and the inhabited regions of the western rim of the SIO basin are particularly prone to repeated TC impacts. Annually, approximately 55% of TCs in the Southern Hemisphere (SH) are formed in the SIO, which spans a large area from the western Indian Ocean to the northwestern coast of Australia [*Ramsay et al.*, 2012]. Thus, improving our understanding of how large-scale climate features control the geneses and tracks of TCs in the SIO is of significant importance.

[1]State Key Laboratory of Earth Surface Processes and Resource Ecology, Beijing Normal University, Beijing, China.
[2]Beijing Meteorological Bureau, Beijing, China.
[3]Korea Polar Research Institute, Incheon, South Korea.
[4]Academy of Disaster Reduction and Emergency Management, Ministry of Civil Affairs and Ministry of Education, Beijing Normal University, Beijing, China.

Corresponding author: R. Mao, State Key Laboratory of Earth Surface Processes and Resource Ecology, Beijing Normal University, Beijing 100875, China. (mr@bnu.edu.cn)

[3] Many studies have analyzed the relationship between climatic factors and TC activities in the SIO. On the interannual time scale, the El Niño–Southern Oscillation (ENSO) was suggested to be important for TC genesis and passage in the SIO [e.g., *Ho et al.*, 2006; *Camargo et al.*, 2007; *Kuleshov et al.*, 2009; *Ash and Matyas*, 2012; *Ramsay et al.*, 2012; *Werner et al.*, 2012]. Through cluster and composite analyses, these studies found that the ENSO is able to modulate large-scale fields in association with TC genesis in the SIO. During El Niño periods, the TC genesis is shifted westward and enhanced west of 75°E, which corresponds to a westward shift of convection [*Ho et al.*, 2006]. On the intraseasonal time scale, the Madden–Julian Oscillation (MJO) has been shown to exert a significant impact on the TC activities in the SIO, although the modulations observed have been found to be sensitive to the definition of the MJO [e.g., *Hall et al.*, 2001; *Bessafi and Wheeler*, 2006; *Ho et al.*, 2006; *Camargo et al.*, 2009; *Ramsay et al.*, 2012]. *Bessafi and Wheeler* [2006] found that TCs are 2.6 times more likely to form in the active phase of the MJO compared with its inactive phase. *Hall et al.* [2001] showed that the influence of the MJO on TC formation is even more pronounced over the Australian region, particularly to the northwestern coast of Australia between approximately 90°E and 120°E, where large differences in the TC genesis rate are linked with the active and inactive phases of the MJO.

[4] In addition to the ENSO and the MJO, some authors have investigated local signals originating from the Indian Ocean, which are associated with changes in the TC activities

in the SIO. In the Indian Ocean's climate, the Indian Ocean dipole (IOD) mode is thought to be important, particularly in combination with anomalously low sea surface temperatures (SST) off Sumatra and high SST in the western Indian Ocean [*Saji et al.*, 1999]. *Werner et al.* [2012] removed the ENSO-related variations from the IOD time series and evaluated the ENSO-independent IOD contribution to TC genesis north of Australia. The ENSO-independent IOD correlates most strongly with TC genesis in the Australian region from August to October prior to the upcoming TC occurrence season with a correlation coefficient of -0.45, which is significant at the 99% confidence level. In addition, *Ash and Matyas* [2012] analyzed the TC trajectories in the southwestern Indian Ocean and found that an interaction between the ENSO and the IOD influences certain types of TC tracks. All of these studies conclude that the ENSO, the MJO, and the IOD modulate the TC activities in the SIO on the intraseasonal to interannual time scale.

[5] As the prominent mode of climatic variability across the SH, the Antarctic Oscillation (AAO) is characterized by pressure anomalies of one sign centered over Antarctica and anomalies of the opposite sign centered at approximately 40°S–50°S [*Gong and Wang*, 1999; *Thompson and Wallace*, 2000]. A positive (negative) AAO phase is defined as higher (lower) pressure at midlatitudes and lower (higher) pressure in Antarctica. Many studies have examined the relevant impact of the AAO on the TC activity. For example, when the AAO is in a positive phase, more TCs pass through the East China Sea and less TCs pass through the South China Sea [*Ho et al.*, 2005]. The linkage between the AAO and the TC passage in the western North Pacific is determined by an apparent teleconnection pattern in the western Pacific in both hemispheres: a huge anticyclone to the southeast of Australia and a relatively small anticyclone in the East China Sea. Some authors examined the linkage between the AAO and TC genesis in the western South Pacific. For example, during the Austral summer season, an enhanced (depressed) eastward propagating MJO is associated with negative (positive) phases of the AAO, which in turn influences TC formation via deep convection [*Carvalho et al.*, 2005; *Pohl et al.*, 2009]. However, less attention has been given to the study of the AAO signal in TC activities in the SIO. The goals of this study were the following: (1) to investigate changes in TC activities associated with the AAO variations and (2) to understand how the AAO is linked to TC activities using observations and simulations. Because a negative (positive) AAO phase tends to be associated with El Niño periods (La Niña periods) [e.g., *Carvalho et al.*, 2005; *Pohl et al.*, 2009], the effects of ENSO on the TC activities were excluded from our study to clarify the contribution of the AAO on the TC activities in the SIO.

[6] This paper is organized as follows. Section 2 describes the data and method used. Section 3 presents a linkage between the AAO and TC genesis and passage. Section 4 reveals the AAO-related variations in the environmental fields through a genesis potential (GP) index. In section 5, we explored the formation of the AAO-TC links by analyzing various environmental fields, such as ocean heat content and water vapor flux. In section 6, the AAO–atmospheric circulation relationship, which is important in the formation of the AAO-TC links, and its reproducibility in a historical climate simulation are discussed. The major findings of the study are then summarized in section 7.

2. Data and Method

2.1. TC Data

[7] The TC best track data, which were obtained from the International Best Track Archive for Climate Stewardship (IBTrACS), were examined in this study (available online at http://www.ncdc.noaa.gov/oa/ibtracs/index.php). The IBTrACS combines best track data from various Regional Specialized Meteorological Centers and Tropical Cyclone Warning Centers. Each best track record contains the TC center locations and intensities at 6 h intervals. Whereas the IBTrACS data set starts in 1842, we had to use the data from 1979 to 2011 due to the questionable data quality during the presatellite era [*Knaff and Sampson*, 2009]. Although TCs are divided into three stages (tropical depression, tropical storm, and hurricane) depending on their maximum sustained wind speed, every stage of TCs was taken into account in this study. Additionally, TC genesis and passage in the SIO between 40°E–120°E and 0°S–30°S were examined.

[8] To measure the TC activities, we defined three indices: TC frequency (TCF), TC genesis frequency (TCGF), and TC passage frequency (TCPF). TCF is the numbers of TCs that initiated in the SIO (40°E–120°E and 0°S–30°S) during the analysis period. To describe the spatial distribution of TC genesis and passage, during a TC lifetime, each center from genesis to lysis was binned into the corresponding 5×5 grid box, and a TC was only counted once even if it entered the same grid box several times. This procedure was repeated for each TC in the SIO during the analysis period. Consequently, the TCGF (TCPF) is the accumulated numbers of TC geneses (centers) in a specific grid box, and each grid box has a value of TCGF (TCPF) (see *Ho et al.* [2005, 2006] and *Choi et al.* [2012] for details). Afterward, a time series of TCF in the SIO and the time series of the TCGF and TCPF for each grid box were constructed during the analysis period.

2.2. ERA-Interim Reanalysis and Ocean Heat Data

[9] The ERA-Interim data set was used not only for the construction of the AAO index but also for the atmospheric circulation analysis. This data set provides many thermodynamic and dynamic variables, such as horizontal winds, relative humidity, specific humidity, relative vorticity, sea level pressure (SLP), and geopotential height, with a 1.5° horizontal resolution and at 37 vertical pressure levels [*Dee et al.*, 2011]. The ocean heat data used in this study corresponded to the SST and the thermocline depth. The SST was obtained from the Met Office HadISST starting from 1979 to 2011 with a spatial resolution of 1°. We used the 20°C isothermal depth (Z20 hereafter) as a proxy for measuring the thermocline depth, which was obtained from a simple ocean data assimilation product [*Carton et al.*, 2000].

2.3. AAO, ENSO, and IOD Indices

[10] The AAO index is defined as the time series of the first leading mode from the empirical orthogonal function analysis using monthly SLP in the ERA-Interim data set [*Gong and Wang*, 1999]. Alternatively, the AAO index is defined as the difference in the normalized monthly zonal mean SLP between midlatitudes and high latitudes based on the reanalysis data set and observations [*Gong and Wang*, 1999; *Marshall*, 2003; *Nan and Li*, 2003]. These AAO indices are nearly identical, and their correlation coefficients are greater

than 0.95. Thus, the usage of these different AAO indices does not alter the present results. To emphasize the interannual variability of the AAO during the analysis, a detrended time series of the AAO index was utilized as the AAO index.

[11] The ENSO years were selected based on information from the Climate Prediction Center (CPC) of the National Oceanic and Atmospheric Administration (http://www.cpc.ncep.noaa.gov/products/analysis_monitoring/ensostuff/ensoyears.shtml). During the TC seasons, there are 10 El Niño periods (1982/1983, 1986/1987, 1987/1988, 1991/1992, 1994/1995, 1997/1998, 2002/2003, 2004/2005, 2006/2007, and 2009/2010) and 10 La Niña periods (1983/1984, 1984/1985, 1988/1989, 1995/1996, 1998/1999,1999/2000, 2000/2001, 2005/2006, 2007/2008, and 2010/2011). In climate simulations, the ENSO years were determined using the means of the monthly Niño 3.4 SST anomalies, i.e., the mean of the SST anomalies over the area of 5°N–5°S and 170°W–120°W. To remove the warming trend in the SST, we utilized the CPC method by calculating the SST departure from the average using 30 year moving base periods. Details are shown at the following website: http://www.cpc.ncep.noaa.gov/products/analysis_monitoring/ensostuff/ONI_change.shtml. The IOD index is represented by the anomalous SST gradient between the western equatorial Indian Ocean (50°E–70°E and 10°S–10°N) and the southeastern equatorial Indian Ocean (90°E–110°E and 10°S–0°S) [*Saji et al.*, 1999].

2.4. Genesis Potential Index

[12] To measure the contribution of thermodynamic and dynamic fields to the TC genesis, a genesis potential (GP) index was used in this study. This index, which was initially presented by *Emanuel and Nolan* [2004], is defined as

$$ \mathrm{GP} = \left|10^5 \eta\right|^{\frac{3}{2}} \left(\frac{H}{50}\right)^3 \left(\frac{V_{\mathrm{pot}}}{70}\right)^3 (1 + 0.1 V_{\mathrm{shear}})^{-2} $$

where η is the absolute vorticity at 850 hPa (in s^{-1}), H is the relative humidity (RH) percentage at 600 hPa, V_{pot} is the potential intensity (in m s^{-1}), and V_{shear} is the magnitude of the vertical wind shear between 850 and 200 hPa (in m s^{-1}). This index has been widely applied to assess the influence of the ENSO/MJO on the TC genesis potential [e.g., *Camargo et al.*, 2007, 2009] and to speculate what factor contributes significantly to the TC genesis potential.

2.5. Analysis Method

[13] We have presented climatological features of TCF prior to a further analysis. Figure 1a depicts the monthly numbers of TCs averaged for the 1979–2010 period for the west of SIO (30°E–100°E and 0°S–30°S) and the northwestern coast of Australia (100°E–120°E and 0°S–30°S), respectively. Generally, the monthly distributions of TCF for both regions are similar. The occurrence of TCs exhibits a peak from December through March (DJFM), which was revealed by *Ho et al.* [2006], *Ramsay et al.* [2012], and *Werner et al.* [2012]. In the west of SIO (the northwestern coast of Australia), more than 2 (0.8) TCs per month are generated in the months of DJFM, 1 (0.25) TC for April and November, and few TCs in the remaining months. As a summary of these statistics, more than two thirds of the total TCs formed over the SIO are observed in the DJFM period. Consequently, the TCs in DJFM over the SIO were analyzed in this study. In turn, the time series of the DJFM TCF/TCGF/TCPF is the sum of the

monthly TCF/TCGF/TCPF in the DJFM period, and the time series of the AAO/ENSO/IOD indices during the DJFM period were determined by averaging the monthly values during the period of DJFM, respectively.

[14] The linkage between the AAO and the TC activity in the SIO was first measured using the Spearman rank correlation, which is a more robust and resistant method compared with the Pearson correlation [*Wilks*, 2006]. This type of correlation is particularly suitable when outliers or observations are not normally distributed. Furthermore, to analyze the AAO-related anomalies in the TCGF/TCPF and the GP index, composites were employed (positive AAO years minus negative AAO years). Due to the low numbers of AAO extreme years (after excluding the ENSO years in the AAO time series) and the scarce records in the TCGF/TCPF for a specific grid box, the statistical significance for the composite analysis was tested using the Wilcoxon unsigned-rank test rather than the paired Student's *t* test because these variables cannot be assumed to be normally distributed. The Wilcoxon unsigned-rank test is a nonparametric statistical hypothesis test that can be used as an alternative to the paired Student's *t* test when the population does not follow a normal distribution.

[15] Because climates over the Indian Ocean and its rims are largely impacted by the ENSO and the IOD [e.g., *Saji et al.*, 1999; *Schott et al.*, 2009], it is essential to consider the ENSO and IOD signals in the composite analysis of the AAO-TC links. As a result, the ENSO years were excluded from the time series of the AAO index, and we then selected the extreme AAO cases as those in which the absolute value of the AAO index was less than 0.5 units. The identified strongly positive AAO cases include the years 1980, 1981, 1989, 1993, and 1996, and the negative AAO cases are 1979, 1992, and 2003. On the contrary, due to the low correlation between the IOD index and the TCF (see section 3.1), the IOD signal was not taken into account in the composite analysis of the AAO-TC links.

3. Relationship Between the AAO and the TC Activity

3.1. Correlation Between the AAO and the TCF

[16] Considering a possible lag effect of the AAO on the DJFM TC activity in the SIO, we first computed the correlation between the preceding AAO index and the DJFM TCF (Figure 1b). In August, September, and October, the AAO has an inverse relationship with the DJFM TCF with a negative correlation, but from November to March, the AAO has a positive correlation with the DJFM TCF. We averaged the AAO index during the DJFM period and then calculated its correlation with the DJFM TCF. The correlation coefficient is 0.37 and is significant at the 95% confidence level. Because the AAO index can be defined by multiple methods, the correlation between the AAO and the DJFM TCF was also calculated with different AAO indices. The results show that the correlation coefficient is 0.37 for the *Gong and Wang* [1999] index, 0.37 for the *Nan and Li* [2003] index, and 0.40 for the *Marshall* [2003] index, and all of these are significant at the 95% confidence level. This finding implies that the positive correlation between the AAO index and the TCF during the DJFM period is independent of the AAO index used. In addition, we compared the extreme values in the time series of
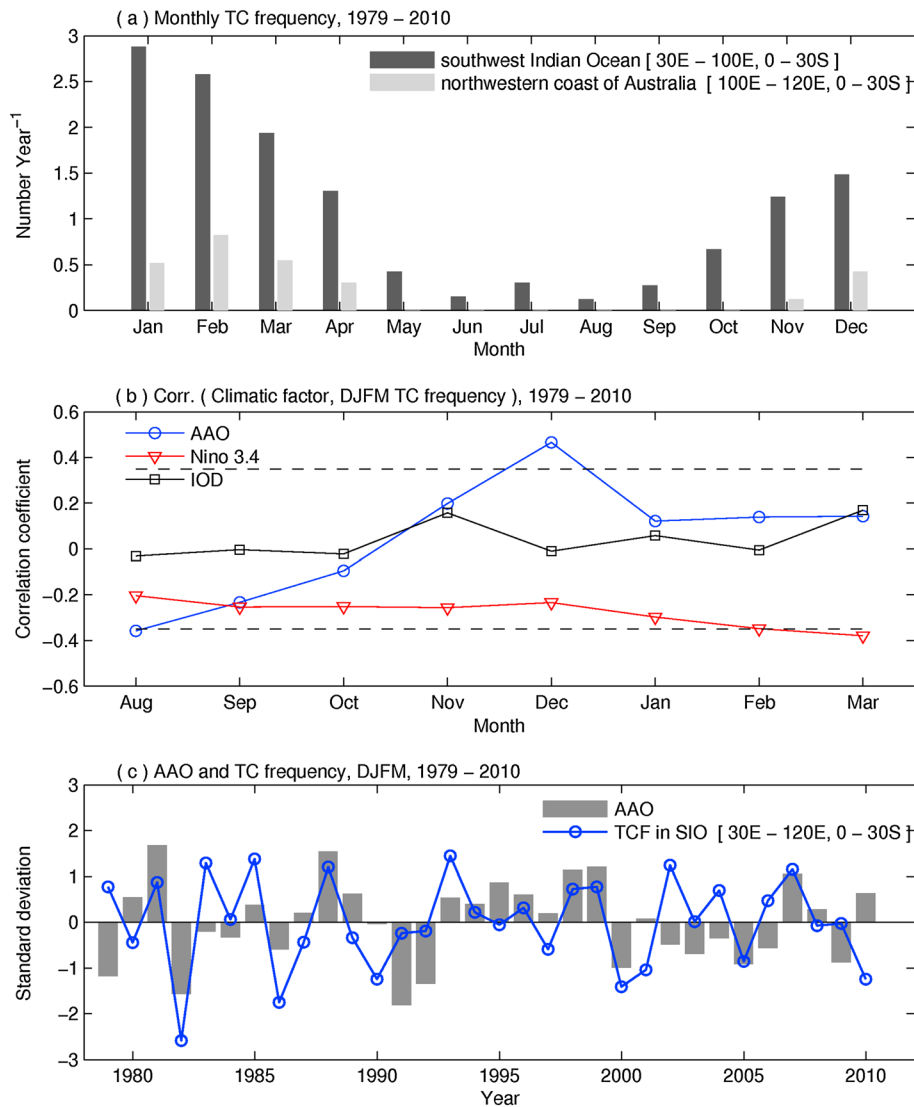
Figure 1. (a) Number of TCs formed each month in the southwest Indian Ocean (SIO, 0°S–30°S and 30°E–100°E) and the northwestern coast of Australia (0°S–30°S and 100°E–120°E) for the period of 1979–2010. (b) Correlations between leading monthly climatic variable and following TC frequency during December–March in the SIO (0°S–30°S and 30°E–120°E). Dashed lines in Figure 1b indicate the 95% confidence level. (c) Standard deviation of the AAO index and TC frequency during the DJFM period in the SIO for the period of 1979–2010.

the TCF and the AAO during the DJFM period (Figure 1c). The five highest-AAO years (1981, 1988, and 1998, 1999, and 2007) have a relatively higher TCF, and four out of the five lowest-AAO years (1982, 1991, 1992, and 2000) have a relatively lower TCF. This finding implies that an increasing (decreasing) TCF tends to be associated with a positive (negative) AAO phase during the DJFM period. In the following section, therefore, we mainly investigated the AAO-TC links during the DJFM period.

[17] In addition to the AAO, we examined the correlation between the preceding ENSO/IOD index and the DJFM TCF (Figure 1b). The ENSO exhibits an evident impact on the DJFM TCF with significant negative correlation coefficients of less than −0.2 during August–March; the minimum value for the correlation coefficient is obtained in March. We averaged the ENSO index during the DJFM period and calculated its correlation with the DJFM TCF; the correlation

coefficient is −0.33 and is significant at the 93% confidence level. These relatively high correlations between the ENSO index and the TCF provide additional evidence that the ENSO signal should be excluded when considering the AAO-TC links in the SIO. On the contrary, the IOD signal has not been excluded during the analysis of the AAO-TC links in the SIO. The correlation coefficients of the proceeding IOD index with the DJFM TCF vary in values from −0.03 to 0.16 for the period of August–March. During the mature phase of the IOD from August to October [*Saji et al.*, 1999], the correlation coefficient between the IOD index and the DJFM TCF is −0.02, which is not significant. These findings indicate that the IOD signal has a weak effect on the DJFM TCF in the SIO, and therefore, the IOD signal was not considered in the subsequent analyses.

[18] Many studies have indicated that a negative (positive) AAO phase tends to be associated with El Niño periods
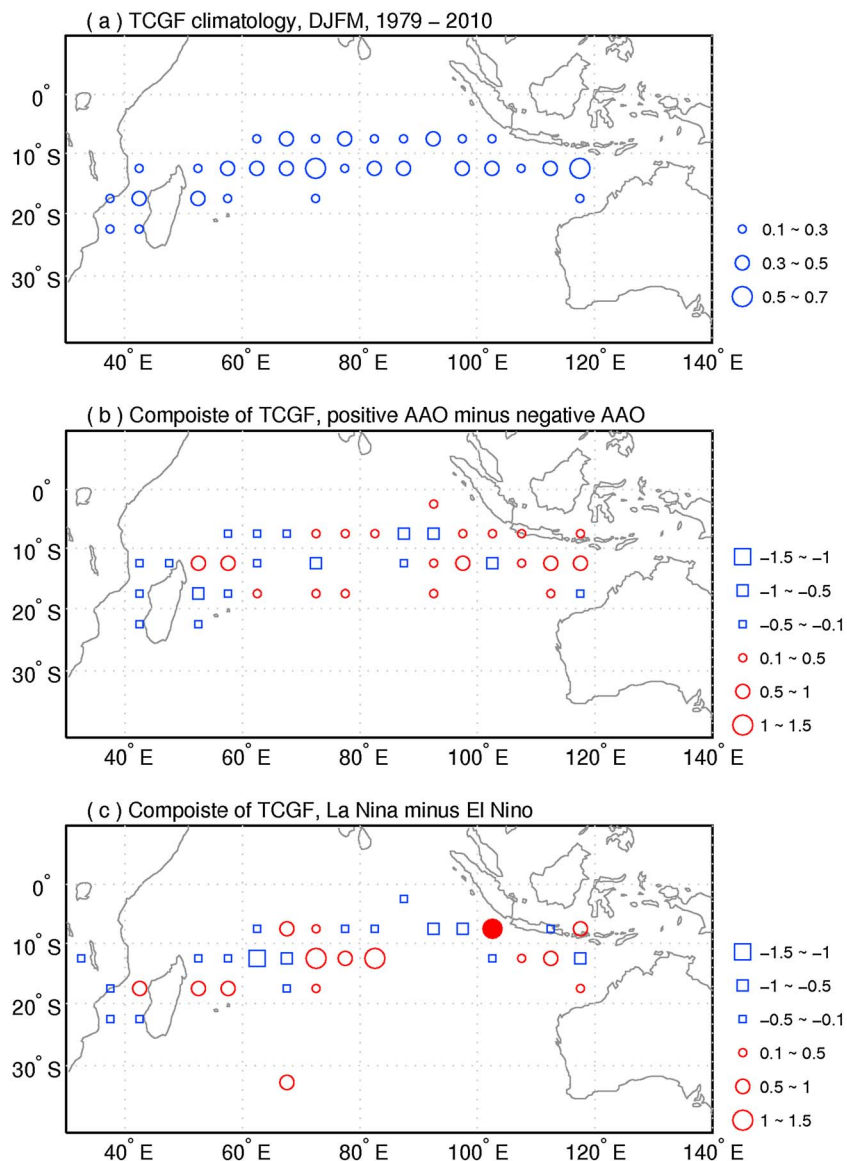
Figure 2. (a) Climatological distribution of TC genesis frequency (TCGF) in December–March (DJFM) for the period of 1979–2010. (b) The difference of DJFM TCGF between positive AAO phases and negative AAO phases (positive AAO minus negative AAO). (c) Same as Figure 2b except for the ENSO episodes (La Niña years minus El Niño years). Circle (square) indicates positive (negative) anomaly in Figures 2b and 2c. Shaded markers are significant at the 90% confidence level.

(La Niña periods) [e.g., *Carvalho et al.*, 2005; *Pohl et al.*, 2009]. It is obvious that the high correlation between the AAO and the TCF during the DJFM period may be caused by the high correlation between the ENSO and the TCF. Thus, we calculated a partial correlation between the AAO and the TCF as the ENSO was maintained constant; the rank partial correlation between the AAO and the TCF was found to be 0.22. In addition, we calculated a rank partial correlation between the ENSO and the TCF during DJFM as the AAO was maintained constant. The partial correlation between the ENSO and the DJFM was -0.15. The comparison of the partial correlations of the AAO and the ENSO revealed that their linkages to the TCF are comparable, although they are both insignificant. On the basis of the analysis above, the impact of the AAO on the TCF in the SIO may be noteworthy, though the impact of the ENSO on the TCF in the SIO

is not negligible. Therefore, it is essential to discuss the AAO-TC linkage in the SIO during the DJFM period.

3.2. AAO-Related Anomalies in the TCGF and the TCPF

[19] In this section, composites of the TCGF and the TCPF during the DJFM period were analyzed (positive AAO years minus negative AAO years). Figures 2a and 2b show the climatology of the TCGF and the AAO-related TCGF anomalies during the DJFM period, respectively. Climatologically, TCs are mainly formed in the region of 50°E–120°E and 5°S–15°S, and a few are formed in the Mozambique Channel. In particular, an average of one TC every 2 years has formed in the following two contracted areas: 55°E–75°E, 5°S–15°S and 100°E–120°E, 10°S–15°S. The composite of the TCGF demonstrates a significantly increasing region located south

Table 1. Correlation Coefficients of the AAO Index and the TC Frequency in the Northwestern Coast of Australia With the Specific Humidity, the OLR, the Height, and the Relative Vorticity Over the Northwestern Coast of Australia[a]

	TC Frequency	Specifc Humidity	OLR	Height	Relative Vorticity
AAO index	0.49[b]	0.37[c]	−0.35[c]	−0.57[b]	−0.57[b]
TC frequency	–	0.41[b]	−0.41[b]	−0.53[b]	−0.27

[a]All time series of variables, except the AAO index and the TC frequency, are computed by averaging values over 10°S–30°S and 100°E–120°E. Specific humidity is averaged between the surface and the 500 hPa level. Relative vorticity and height are calculated as specific humidity but between 850 and 500 hPa levels.

[b]Significant at the 99% level.

[c]Significant at the 95% level.

of 10°S and east of 100°E and an evident decreasing area centered to the northeast of Madagascar when the AAO is in a positive phase. Compared with the climatological TCGF, the magnitude of the anomaly corresponds to an approximately 100% fluctuation, although these results are not significant at the 90% confidence level due to the low numbers of extreme years analyzed. We constructed a time series of the TCF in the northwestern coast of Australia during the DJFM period and calculated its correlation with the DJFM AAO index. The correlation coefficient is 0.49, which is significant at the 99% confidence level (Table 1). This high correlation coefficient reveals a tight AAO-TC linkage in the northwestern coast of Australia.

[20] Figures 3a and 3b show the climatology of the TCPF and the AAO-related TCPF anomalies during the DJFM period. The TC passages during the DJFM period mainly spread south of 10°S and accompany a dipole distribution:
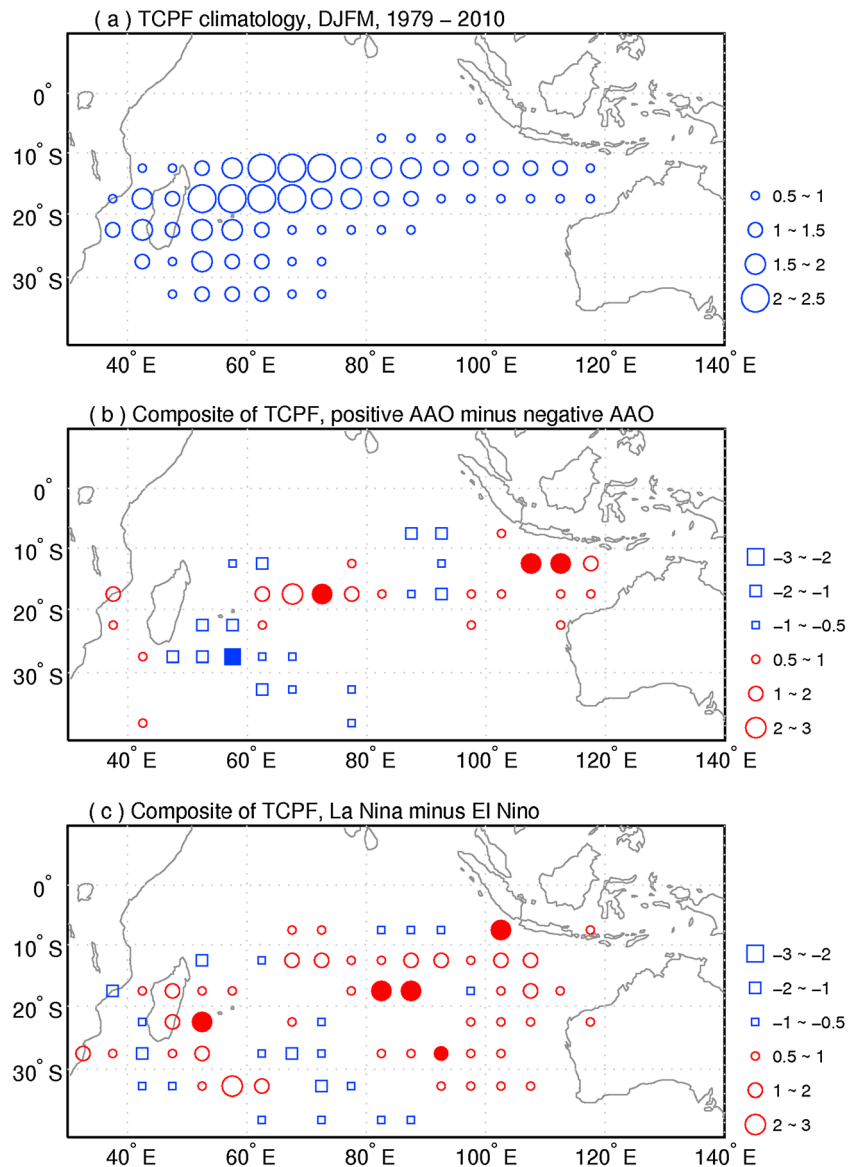
Figure 3. Same as Figure 2 except for the TC passage frequency (TCPF).
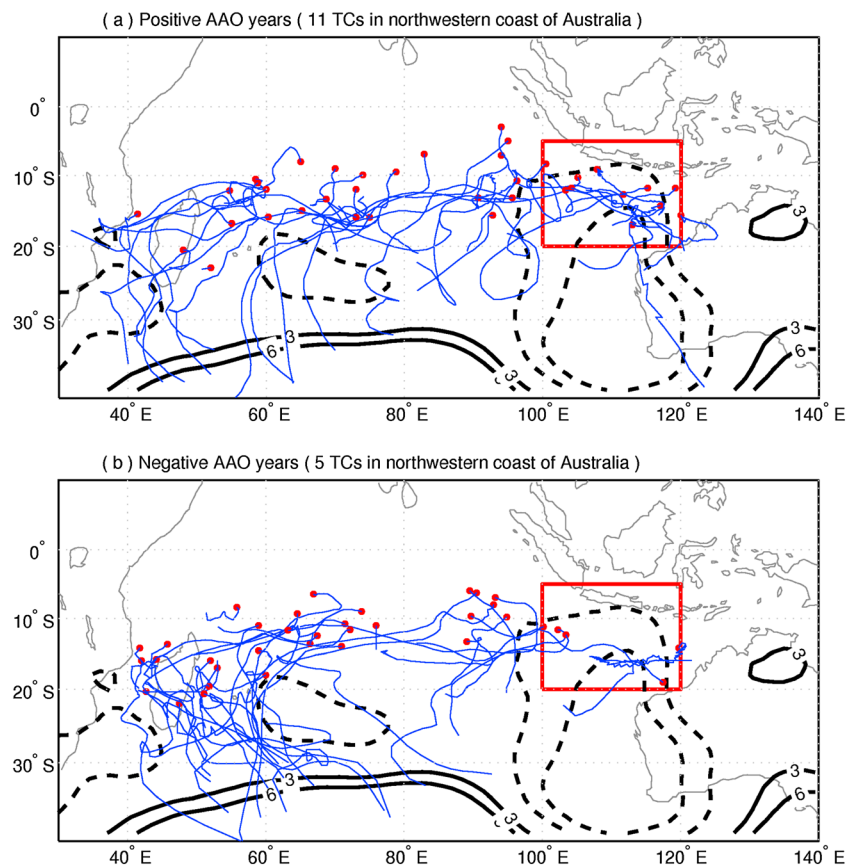
Figure 4. Best tracks of all tropical cyclones in the period of December–March (DJFM) for (a) the highest-AAO years (1981, 1989, and 1996) and (b) the lowest-AAO years (1979, 1992, and 2003). Red points indicate the locations of TC geneses, and blue lines denote TC tracks. Contours show the difference of height in the low to middle troposphere (averaged between 850 and 500 hPa) between the highest-AAO years and the lowest-AAO years during DJFM (positive AAO years minus negative AAO years; unit: meters). Positive (negative) anomalies are contoured with solid (dashed) lines. The red box corresponds to the region of the northwestern coast of Australia.

one is located west of 90°E, and the other is found in the northwestern coast of Australia. The average TCPF over these regions are higher than 1.5, which implies that these regions suffer at least one or two TC activities per year. The composite of the TCPF presents positive anomalies in a double structure: one in the northwestern coast of Australia (100°E–120°E and 10°S–30°S) and one in the 60°E–85°E and 15°S–20°S region. The increase in the TCPF in the northwestern coast of Australia provides additional confidence for the increase in the TCGF in that region. Although few grid boxes in the northwestern coast of Australia, where the TCPF exhibits increasing anomalies, satisfy the statistical significance at the 90% confidence level, due to the small numbers of analyzed years, these increasing anomalies correspond to an approximately 100% fluctuation from the climatology. Meanwhile, the composite of the TCPF shows significant decreasing TCPF to the southeast of Madagascar around 45°E–70°E and 20°S–30°S when the AAO is in a positive phase. These negative anomalies also correspond to an approximately 100% fluctuation from the climatology.

[21] To confirm the relationship between the AAO and the TCGF/TCPF, the tracks of TCs were depicted for the three highest-AAO years (1981, 1989, and 1996; Figure 4a) and the three lowest-AAO years (1979, 1992, and 2003; Figure 4b).

In general, the accumulated TCF in the northwestern coast of Australia is higher during the positive AAO years (11 TCs) than during the negative AAO years (5 TCs). In addition, compared with the TCs in the negative AAO years, less TCs pass through the southeastern coast of Madagascar when the AAO is in a positive phase, which is consistent with the decreasing TCPF in Figure 3b. The decreasing TCPF in the southeastern coast of Madagascar is related to the negative height anomaly to the east of that region during the positive AAO phases. This negative height anomaly is accompanied by anomalous southeasterly winds (see details in Figure 9b), which inhibits TCs to move across the southeastern coast of Madagascar.

3.3. ENSO-Related Anomalies in the TCGF and the TCPF

[22] In order to compare the contribution of the AAO and the ENSO to the TCGF and TCPF in the northwestern coast of Australia, composites of TCGF and TCPF for ENSO episodes were analyzed. To exclude the AAO signal in the composite analysis of the ENSO-TC links, we selected the extreme ENSO cases as those in which the AAO index is lower than 0.5 units and larger than −0.5 units. The identified El Niño episodes include the years 1987, 1994, 1997, 2002, and 2004, and the identified La Niña episodes are 1983 and 1984.
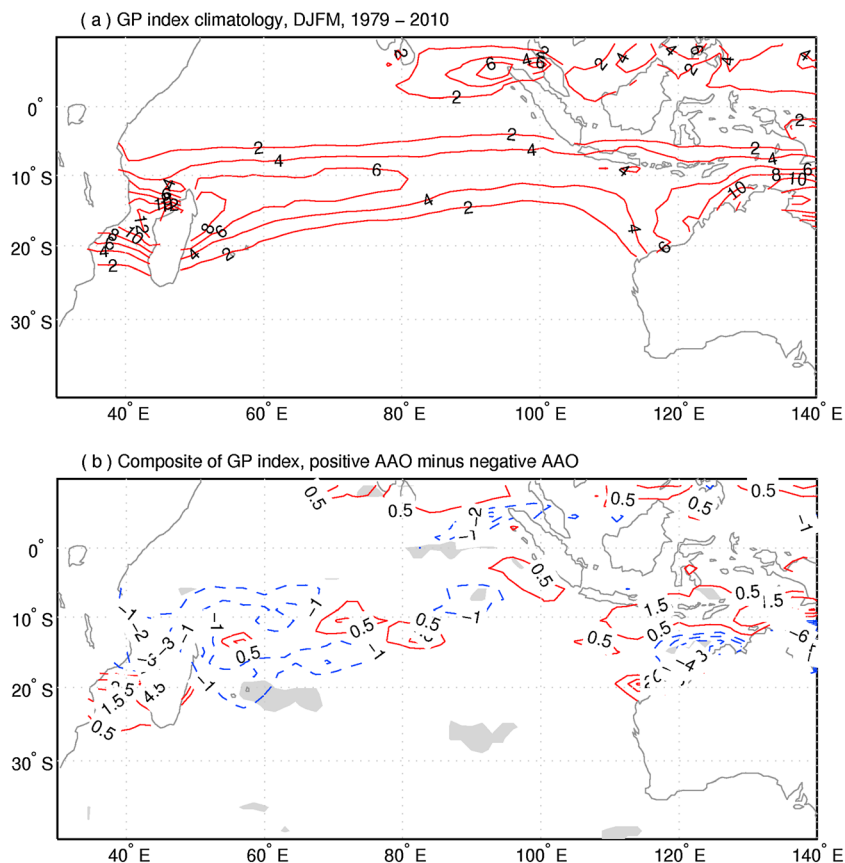
Figure 5. (a) Climatological distribution of genesis potential index during December–March. (b) The difference of genesis potential index between positive AAO phases and negative AAO phases. Shaded areas are significant at the 90% confidence level.

[23] Figure 2c presents the composite of the TCGF for the ENSO episodes (La Niña years minus El Niño years). During the La Niña episodes, an increase of TC genesis is observed in the area located off the northwestern coast of Australia and in the region centered around 70°E–85°E and 10°S–15°S, which are consistent with the findings of *Ho et al.* [2006] and *Kuleshov et al.* [2009]. Compared with the AAO-related anomalies of TCGF (Figure 2b), the La Niña episodes as well as the positive AAO phases may contribute to the increasing TC geneses in the northwestern coast of Australia.

[24] Figure 3c shows the composite of the TCPF for the ENSO episodes. During La Niña episodes, positive TCPF anomalies prevail in the east of SIO and in the southeastern coast of Madagascar. Meanwhile, negative TCPF anomalies are located in the central southern SIO around 60°E–80°E and 20°S–35°S. The comparison of the AAO- and ENSO-related TCPF anomalies reveals that the ENSO signal is a dominant factor in modulating TC passage in the east of SIO, in particular between 80°E and 110°E; however, the impact of AAO on the TC passage in the northwestern coast of Australia is noteworthy, which is comparable to the impact of ENSO on the TC passage in that region.

4. Relationship Between the AAO and the Genesis Potential Index

[25] Although the above analysis reveals the AAO-TC links in the SIO, particularly in the northwestern coast of Australia,

the mechanism responsible for the observed linkages is not clear. TC genesis is responsible for TC formation and is thought to be influenced by a number of large-scale environmental factors. Understanding the influence of these large-scale environmental factors on the TC genesis is of great scientific importance. Recently, the GP index, which was introduced by *Emanuel and Nolan* [2004], has been widely employed in TC studies to assess which environmental factors contribute to the TC genesis associated with the ENSO/MJO variations [*Camargo et al.*, 2007, 2009]. Therefore, the relationship between the AAO and the GP index will be examined in the context of the AAO-TC links in the SIO.

4.1. Composite of the Genesis Potential Index

[26] Figure 5a shows the climatology of the GP index during the DJFM period in the SIO. The figure shows a high-GP-index band from Madagascar to the northwestern coast of Australia with two peaks: one occurring around Madagascar (40°E–80°E and 10°S–20°S) and the other located in the northwestern coast of Australia. Compared with Figure 2a, the GP index is able to reproduce the climatological TCGF, i.e., a high TCGF was found in both the northwestern coast of Australia and the region between 40°E–80°E and 10°S–20°S.

[27] Figure 5b presents the composite of the GP index. When the AAO is in a positive phase, there are three areas that exhibit a positive anomaly of the GP index: one in the northwestern coast of Australia, one in the region between

Composite of GP index for varying variable (positive AAO minus negative AAO)
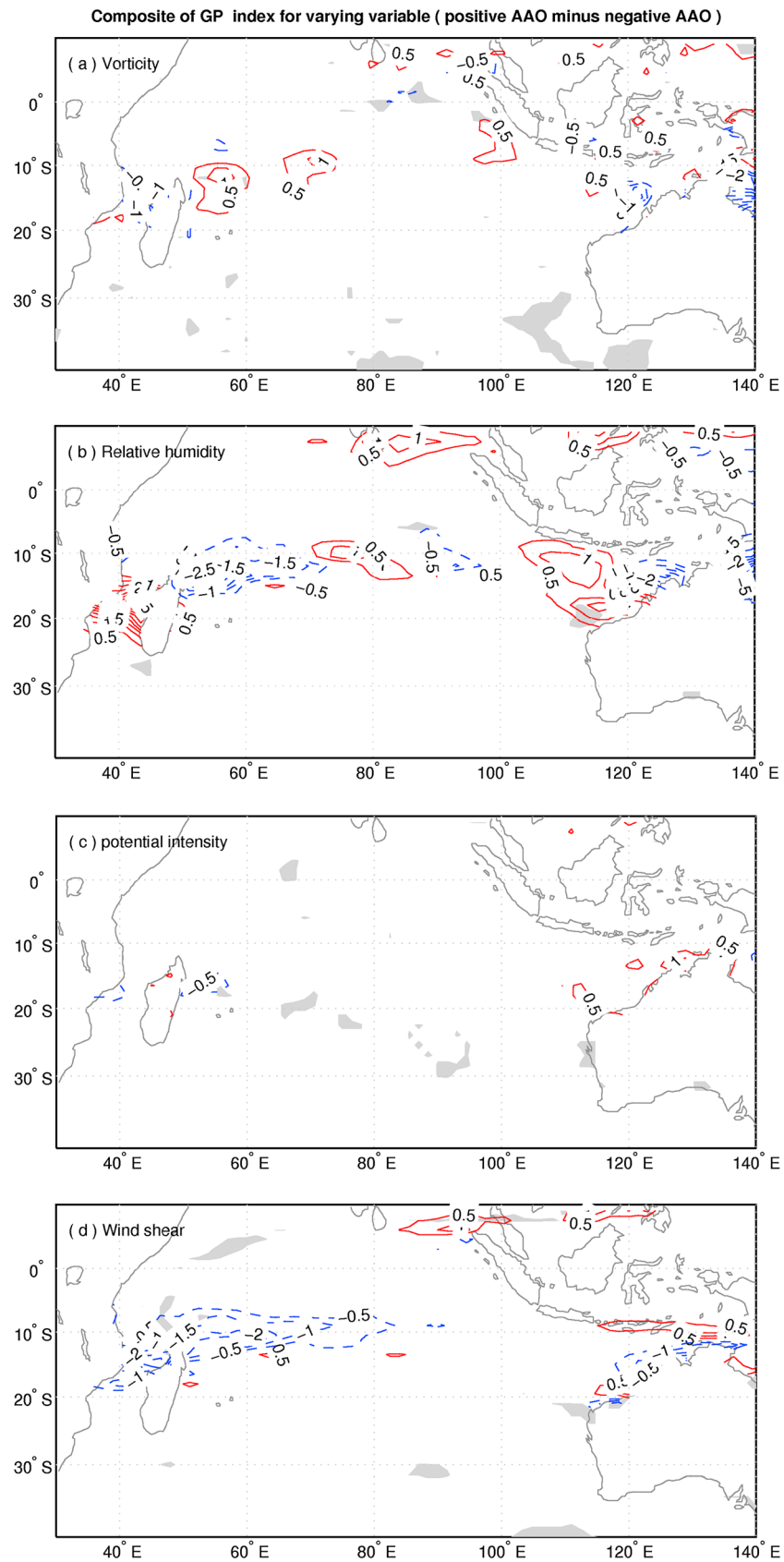
Figure 6. Difference of genesis potential index between positive AAO phases and negative AAO phases during the period of December–March for varying (a) low-level absolute vorticity, (b) relative humidity, (c) potential intensity, and (d) vertical wind shear with the other variables as climatology. Shaded areas are significant at the 90% confidence level.
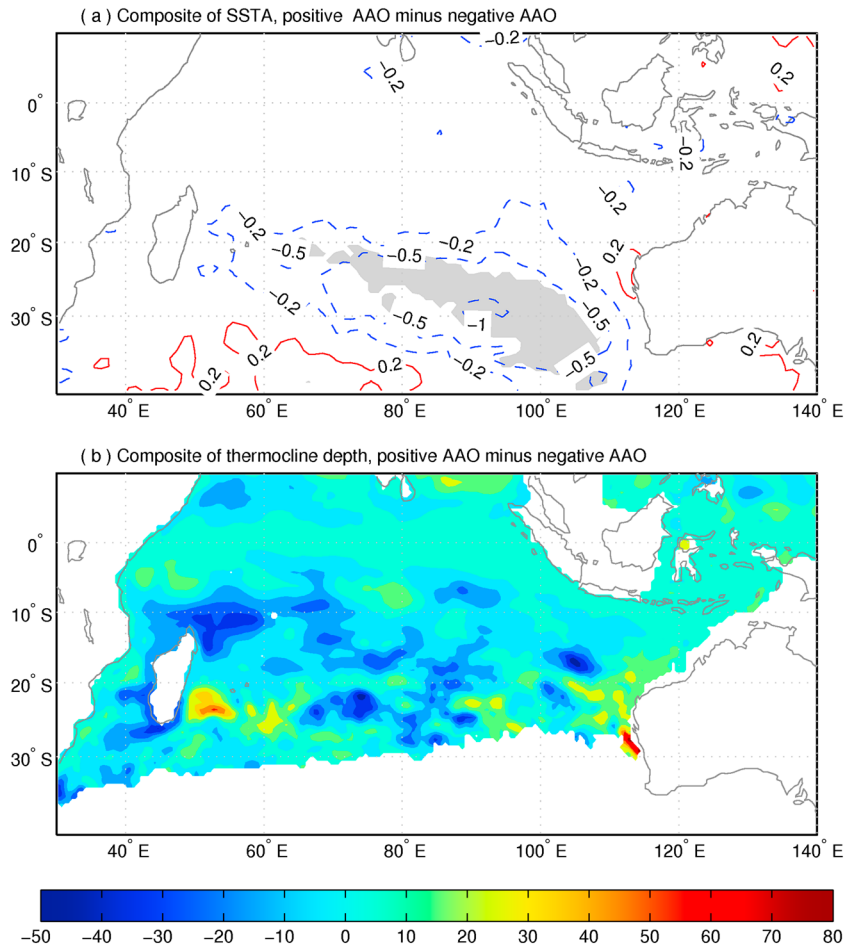
Figure 7. (a) Difference of sea surface temperature between positive AAO phases and negative AAO phases during the period of December–March. (b) Same as Figure 7a except for thermocline depth. In Figure 7a, positive (negative) anomalies are presented by solid (dashed) lines, and shaded areas are for values significant at the 90% confidence level. The units are degrees Celsius and meters in Figures 7a and 7b, respectively.

70°E and 90°E at 10°S, and one between 55°E–60°E and 10°S–15°S. The negative anomaly of the GP index spans the area between 50°E–70°E and 5°S–20°S, which surrounds the positive anomaly of the GP index between 55°E–60°E and 10°S–15°S. In general, the composite of the GP index nearly reproduces the AAO-related TCGF anomalies. The positive anomalies of the GP index and the TCGF are colocated in the northwestern coast of Australia, the region between 70°E–85°E and 5°S–10°S and the region between 50°E–65°E and 10°S–15°S. Meanwhile, the negative anomalies of the GP index reproduce the anomalous negative TCGF anomalies prevailing in the northeastern coast of Madagascar. Therefore, the GP index provides an objective description for the TC genesis potential and its changes associated with the AAO variations.

4.2. Factors Influencing the AAO-TC Links

[28] As mentioned previously, the GP index is composed of four variables: vorticity, vertical wind shear, potential intensity, and relative humidity (RH). It is interesting to examine which factors are responsible for the AAO-TC links. Using the method described by *Camargo et al.* [2007, 2009], we recalculated the GP index using the climatological values

of three of the four variables and unmodified, interannually varying values for the fourth variable. This process was repeated four times; during each repetition, one variable was varied, and the other three variables were unchanged. Then, the composite for each case was calculated according to the AAO extremes. Although the GP index is nonlinear, which implies that the total anomaly does not need to be equal to the sum of the four fields described here, the nonlinearities are small, and the attributions obtained by this method should be meaningful [*Camargo et al.*, 2009].

[29] Figure 6 shows the composite of the GP index for cases of varying vorticity (Figure 6a), RH (Figure 6b), potential intensity (Figure 6c), and vertical wind shear (Figure 6d). In each case, the other three variables were maintained at their long-term climatological values. Comparing these results with the pattern obtained when all four of the factors are varied (Figure 5b), it is apparent that the contributions of different factors to the GP index anomalies shift in different regions. The positive GP index anomalies in both the northwestern coast of Australia and the region between 70°E and 90°E at 10°S are mainly due to the increasing RH at the 600 hPa level. The vorticity, potential intensity, and vertical wind shear contribute less to these positive GP index

(a) Composite of water vapor flux divergence, positive AAO minus negative AAO

(b) Composite of Omega, DJFM, 850 – 500 hPa, positive AAO minus negative AAO
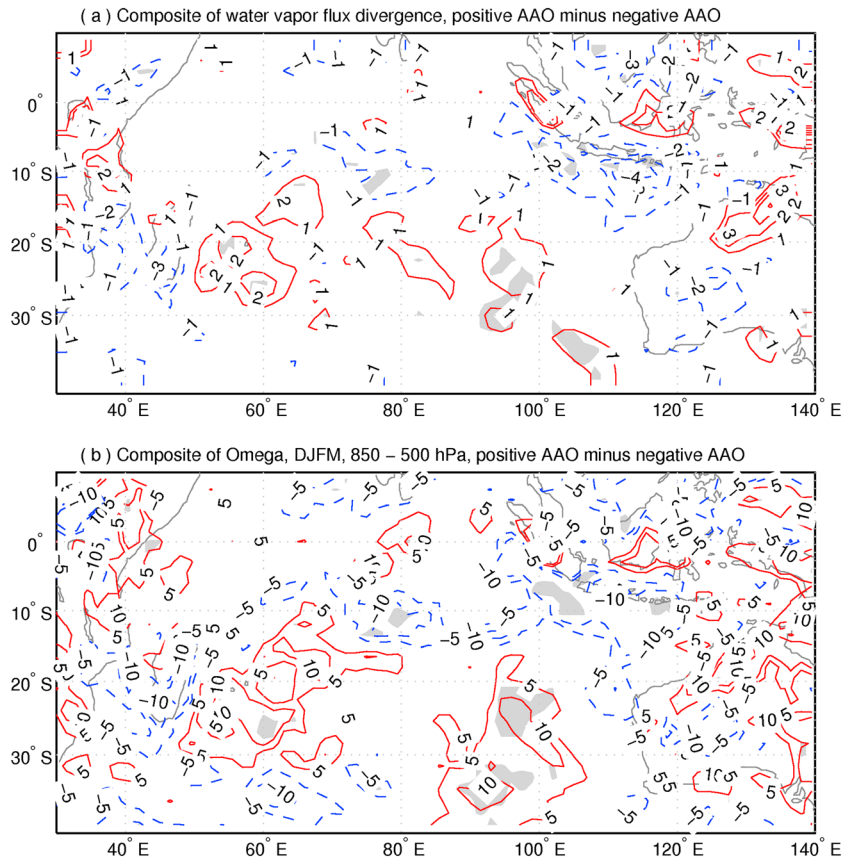
Figure 8. Difference of (a) water vapor flux divergence and (b) vertical motion (omega) between positive AAO phases and negative AAO phases during the period of DJFM. Positive (negative) anomalies are presented by solid (dashed) lines, and values significant at the 90% confidence level are shaded. The units are $10^{-5}\,\mathrm{Kg\,m^{-2}\,s^{-1}}$ and $10^{-3}\,\mathrm{Pa\,s^{-1}}$, respectively, for water vapor flux divergence and vertical motion.

anomalies. These findings suggest that the increase in the TC genesis in the northwestern coast of Australia associated with the high AAO years is mainly the result of changes in the humidity in the middle troposphere, which will be further discussed in the following sections.

[30] Meanwhile, the negative GP index anomalies occurring in the northeastern coast of Madagascar may be related to the vertical wind shear and the RH at the 600 hPa level. To clarify the role of vertical wind shear in these negative GP index anomalies, a composite of vertical wind shear during the DJFM period was analyzed (figure omitted). During the positive AAO phases, increased anomalies of vertical wind shear are located to the northeast of Madagascar. Because enhanced vertical wind shear inhibits TC genesis, the increased anomalies of vertical wind shear to the northeast of Madagascar could be prone to the decreased TCGF in Figure 2b and the negative GP index anomaly in Figure 6d in that region. In addition, to explain the contribution of RH to the negative GP index anomaly in the northeastern coast of Madagascar, the composites of upper ocean heat content during the DJFM period were analyzed (Figure 7). When the AAO is in a positive phase, the decreased thermocline depth to the northeast of Madagascar supports the decreased RH at the 600 hPa level in that area by decreasing evaporation, which could produce the decreased TCGF in Figure 2b and the negative anomalies of GP index in Figure 6d in the northeastern coast of Madagascar.

5. Relationship Between the AAO and the Relative Humidity

[31] The aforementioned results imply that an increased RH at the 600 hPa level may contribute significantly to the increase in the TCGF in the northwestern coast of Australia when the AAO is in a positive phase. In general, above-normal RH tends to occur over/near areas of more-than-normal upper ocean heat storage by high SST and deepened thermocline depth. In addition to the upper ocean heat content, the water vapor flux in the troposphere plays an important role in the formation of a high RH in the troposphere. Therefore, there may be a tight relationship between the AAO and the upper ocean heat content/water vapor flux, which links the AAO to the RH in the troposphere. To clarify this issue, we will examine the AAO-related changes in the upper ocean heat content (SST and thermocline depth) and the water vapor flux in this section.

5.1. AAO-Related Changes in the SST and the Thermocline Depth

[32] We first analyzed the composite of the SST (Figure 7a). In a positive AAO phase, the SST anomalies are generally negative and span from Madagascar southeastward to Australia between 20°S and 40°S. The negative SST anomalies are significant at the 90% confidence level, and the lowest value of less than −0.5°C was found in the western coast of Australia. In addition, positive SST anomalies are found to
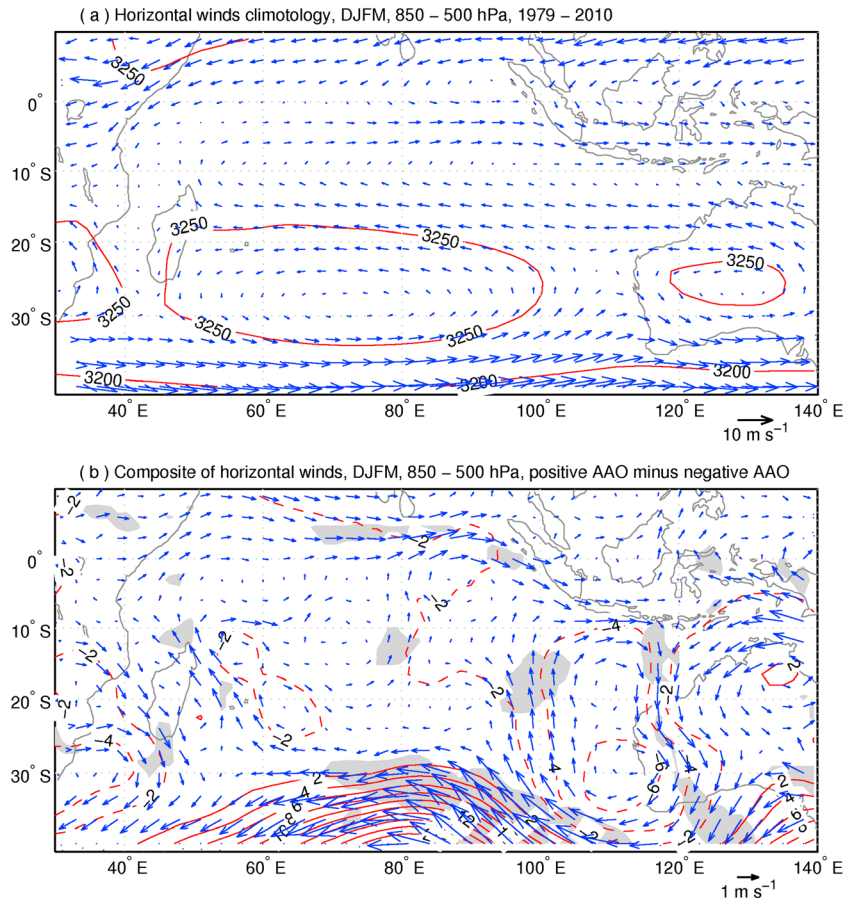
Figure 9. (a) Climatological distribution of horizontal winds (vectors) and height (contour lines) averaged between 850 and 500 hPa during the period of December–March (DJFM). (b) The difference of horizontal winds and height between positive AAO phases and negative AAO phases for the period of DJFM. Shaded areas are significant at the 90% confidence level for horizontal winds in Figure 9b. The units are meters per second and meters for horizontal winds and height, respectively.

the southwest of the negative SST anomalies. The comparison of Figures 2b and 7a demonstrates that the SST alone cannot explain the above-normal RH in the northwestern coast of Australia because there are no obvious SST increases in this region. This inconsistency between the AAO and the SST in the northwestern coast of Australia may be caused by anomalous surface radiation fluxes, including incident solar radiation, latent heat, and sensible heat flux, which are also responsible for the anomalies in the SST [*Gong et al.*, 2013].

[33] We then analyzed the AAO-related changes in the thermocline depth (Z20, Figure 7b). Negative Z20 anomalies are dominant in the SIO when the AAO is in a positive phase, even though positive Z20 anomalies are sparsely scattered in the tropics: one anomaly is located in the northwestern coast of Australia, and the other is found between 5°S–10°S and 70°E–80°E. The comparison of Figures 2b and 7b indicates that the relationship between the AAO and the thermocline depth cannot fully support the AAO-RH links in the northwestern coast of Australia, because the positive Z20 anomalies are weak and cannot explain the existence of a high RH in that area through evaporation.

5.2. Water Vapor Flux

[34] We analyzed the AAO-related changes in the convergence/divergence of the water vapor flux (Figure 8a) in the

lower to middle troposphere. The ERA-Interim reanalysis data set was employed to calculate the column atmospheric water vapor flux, which was integrated vertically from the surface to the 500 hPa level, similarly to the method described by *Zhou and Yu* [2005]. Negative (positive) values indicate that the water vapor is convergent (divergent) and thus prone to high (low) RH in the troposphere. As shown in the figure, when the AAO is in a positive phase, significant negative anomalies in the water vapor flux occur in the northwestern coast of Australia and the region between 5°S–15°S and 70°E–90°E. This result suggests the convergence of water vapor flux over these regions, which contribute significantly to a high RH at the 600 hPa level.

[35] How are these negative anomalies in the water vapor flux formed? To determine the mechanism, we analyzed the AAO-related changes in the water vapor transport using a composite of the water vapor transport (figure not shown; refer to Figure 9b). As shown in the figure, a cyclonic anomaly of water vapor transport is distributed in the northwestern coast of Australia, and its northern branch is located between 5°S–15°S and 100°E–120°E. In addition, westward anomalies in the water vapor transport are found between 5°S–15°S and 120°E–140°E. These two anomalies in the water vapor transport contribute to the water vapor convergence over the northwestern coast of Australia, as revealed by the negative
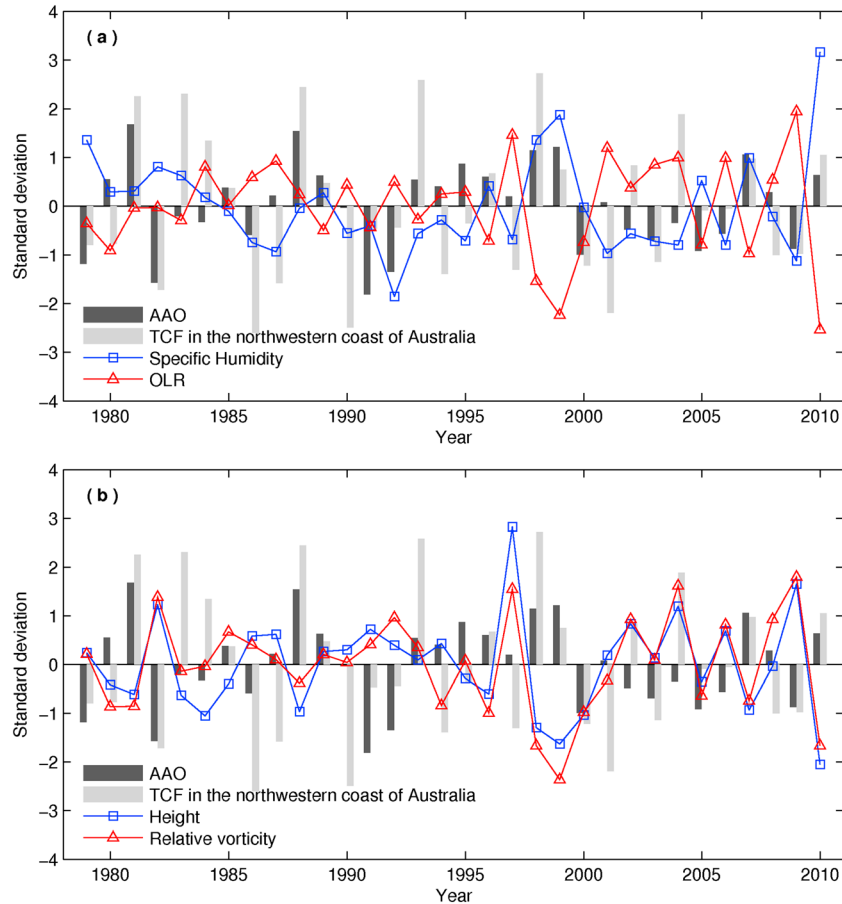
Figure 10. (a) Standard deviations of the AAO index and the TC frequency, the specific humidity, and the outgoing longwave radiation (OLR) in the northwestern coast of Australia (100°E–120°E and 10°S–30°S). (b) Same as Figure 10a except for the height and the relative vorticity in the northwestern coast of Australia. The specific humidity is averaged between the surface and the 500 hPa level. The relative vorticity and height are calculated by averaging values between 850 and 500 hPa levels.

anomalies in the water vapor flux in Figure 8a. Similarly, the negative anomalies in the water vapor flux between 5°S–15°S and 70°E–90°E are produced by the convergence of anomalous water vapor transports (one stretches southeastward and the other flows northwestward), which converge in that region.

[36] In addition to the water vapor flux, we also analyzed the changes in the vertical air motion associated with the AAO variations, because enhanced ascending motions are helpful for the formation of a high RH in the troposphere. Figure 8b shows the composite of vertical air motion. When the AAO is in a positive phase, the ascending motions are coenhanced in the regions where the RH increases: the northwestern coast of Australia and the region between 5°S–15°S and 70°E–90°E. These enhanced ascending motions are nearly colocated with the convergence of the water vapor flux, both of which contribute to the high RH in the troposphere.

6. Discussion

[37] As analyzed previously, during a positive AAO phase, the enhanced RH may be responsible for the increase in the TCGF in the northwestern coast of Australia, and the enhanced RH may be determined by water vapor convergence

and an underlying ascending motion. However, what is the relationship between the AAO and the atmospheric circulation in the SIO? This relationship is essential to the formation of the AAO-RH links. To clarify this issue, we investigated the relationship between the AAO and the height through observations. In addition, if this relationship between the AAO and the height as revealed through observations is true, we would expect a similar linkage in a physical climate simulation. Thus, we examined this relationship through a historical climate simulation using the Community Climate System Model 4 (CCSM4) of the Coupled Model Intercomparison Project Phase 5 (CMIP 5).

6.1. Relationship Between the AAO and the Atmospheric Circulation

[38] To reveal the relationship between the AAO and the atmospheric circulation, we showed that the averaged climatological horizontal winds in the low to the middle troposphere (850–500 hPa) and their composite (positive AAO years minus negative AAO years). Climatologically, two anticyclones occur south of 15°S over the SIO and Australia, respectively, and they exhibit easterly winds between 10°S and 22°S and westerly winds south of 22°S. In addition, westerly winds occur in the tropics between the equator and

10°S (Figure 9a). Figure 9b presents the composites of the horizontal winds and the height. The anomalies in the horizontal winds are nearly colocated with the anomalies in water vapor transport and accompany a cyclonic anomaly in the northwestern coast of Australia and an anticyclonic anomaly over Australia. These circulation anomalies are converged in the northwestern coast of Australia and generate a convergence of water vapor flux, as depicted in Figure 8a. However, an arising question is how the circulation anomalies, particularly the cyclonic anomaly in the northwestern coast of Australia, are generated. The comparison between the AAO-related circulation anomalies and the climatological horizontal winds indicates that the cyclonic circulation anomaly over the northwestern coast of Australia may be caused by the weakening of the climatological anticyclone over Australia. When the AAO is in a positive phase, the anticyclone over Australia becomes weak, moves eastward, and then initiates a cyclonic circulation anomaly to the west of this anticyclone. This cyclonic circulation anomaly is not only prone to the formation of cyclonic vorticity but also beneficial to driving the southerly winds to the east of the climatological anticyclone in the SIO northward to the equator. These enhanced southerly winds transport a high amount of water vapor to the northwestern coast of Australia and result in a high RH in the troposphere in that region.

[39] We then examined the relationship between the AAO and the regional means of the height, the atmospheric moisture, and the relative vorticity over the northwestern coast of Australia (10°S–30°S, 100°E–120°E). The atmospheric moisture is represented by the specific humidity (averaged between the surface and the 500 hPa level) and the outgoing longwave radiation (OLR) [*Liebmann and Smith*, 1996]. During the DJFM period, the correlation between the AAO index and the specific humidity (OLR) over the northwestern coast of Australia is 0.37 (-0.35), which is significant at the 95% confidence level (Figure 10 and Table 1). This result suggests that the high atmospheric moisture in the northwestern coast of Australia is significantly related to a positive AAO phase. In addition, during the DJFM period, the average height and the average relative vorticity over the northwestern coast of Australia exhibit high correlations with the AAO index with correlation coefficients of -0.57, which are significant at the 99% confidence level. These high correlations between the AAO index, the height, the relative vorticity, and the atmospheric moisture imply that the cyclonic circulation anomaly in the northwestern coast of Australia associated with the AAO phases increases the relative vorticity and the atmospheric humidity in the troposphere, which supports the formation of TCs in that region. Furthermore, the correlation between the TCF and the regional means of the height, the atmospheric moisture, and the relative vorticity in the northwestern coast of Australia were computed (Figure 10 and Table 1). The TCF shows a high correlation with the specific humidity (OLR) with the correlation coefficient of 0.41 (-0.41), which is significant at the 99% confidence level and indicates the importance of the humidity to the formation of TCs in that region. Meanwhile, the TCF is significantly correlated with the height with a correlation coefficient of -0.53 at the 99% confidence level, although the TCF has a weak correlation with the relative vorticity with a correlation coefficient of -0.27. Through the analysis above, the high correlations of the AAO and the TCF with the regional means of specific

humidity and height in the northwestern coast of Australia provide additional evidence for the AAO-TC links in that region.

[40] To further examine the relationship between the AAO and the cyclonic circulation anomaly over the northwestern coast of Australia, the changes in the SH height associated with the height fluctuation over the northwestern coast of Australia were analyzed. First, we constructed a time series of the average height over the northwestern coast of Australia (10°S–30°S and 100°E–120°E). Second, to eliminate the effect of the ENSO and the long-term trend in the height, the time series of the average height was detrended, and the ENSO years were then removed from the newly obtained time series. Third, the three highest years were specified as the high-height years (1989, 1990, and 1992), and the three lowest years were specified as the low-height years (1980, 1981, and 1996). Figure 11a shows the composite of the SH height, which is associated with the fluctuation in the height over the northwestern coast of Australia (low-height years minus high-height years). There is an obvious seesaw pattern in the atmospheric pressure and mass formed between the polar region and the middle latitude region, and this pattern is similar to the typical spatial distribution of the positive AAO phase [*Gong and Wang*, 1999] and indicates a negative height anomaly over the northwestern coast of Australia. These height anomalies suggest that the cyclonic height anomaly over the northwestern coast of Australia is significantly related to the positive AAO phase.

6.2. Reproducibility of the AAO-TC Links in a Historical Climate Simulation

[41] If the relationship between the AAO and the height revealed above through observations is true, we would expect a similar linkage in a physical climate simulation. In this section, we examined the reproducibility of this relationship in a historical climate simulation of CCSM4 in CMIP5. We chose CCSM4 because CCSM has exhibited good performance in the simulation of the AAO [e.g., *Zhu and Wang*, 2010; *Zhang*, 2010]. CCSM4 is a fully coupled atmosphere-ocean-sea ice general circulation model [*Gent et al.*, 2011]. The atmosphere component of this model has a horizontal resolution of 1.25° and 17 levels in the vertical direction. Its ocean component has a horizontal resolution of approximately 1°. Details of the CCSM4 model can be found at http://www.cesm.ucar.edu/models/ccsm4.0/. The CCSM4 simulation analyzed here is the first historical run in CMIP 5 forced by varying major greenhouse gases and aerosols. This coupled simulation is performed covering period of 1850–2004.

[42] The AAO index in the simulation was defined using the same method used in the observations and was also detrended. We first examined the simulated SH height anomaly in association with the AAO variation using composite analysis (data not shown). The results show a typical AAO pattern in the SH, which is characterized as approximately zonally symmetric. The pattern shows negative height anomalies centered in Antarctica and positive height anomalies centered at approximately 40°S–50°S over the Pacific, Indian, and Atlantic Oceans. These anomalies are significant at the 90% confidence level. In addition, as we reported through observations, there was only one negative, albeit insignificant, height anomaly at a low latitude over the northwestern coast of Australia.

[43] The changes in the SH height associated with the height fluctuation over the northwestern coast of Australia were also
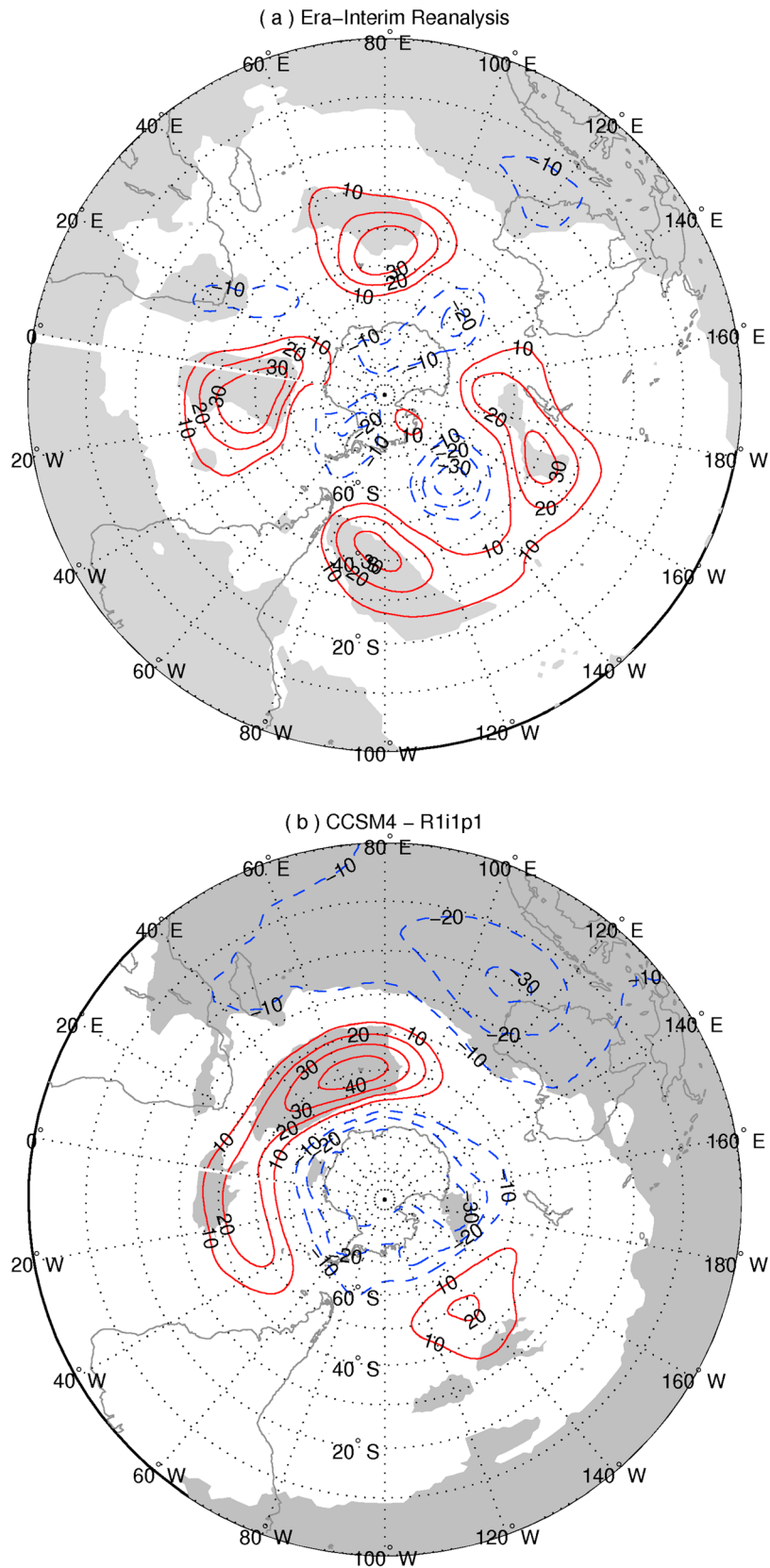
Figure 11. Difference of height in the Southern Hemisphere between the lowest-height years and the highest-height years (low minus high) during the period of December–March, which is calculated by (a) the Era-Interim reanalysis data set and (b) the CCSM 4 simulation. The extreme years of height are determined by the fluctuation of height averaged between 10°S–30°S and 100°E–120°E. Shaded areas are significant at the 90% confidence level.

```
┌─────────────────────────────────────────┐
│           A positive AAO phase            │
└─────────────────────────────────────────┘
                     │
                     ▼
┌─────────────────────────────────────────┐
│  the climatological high over Australia   │
│     weakening and moving eastward         │
└─────────────────────────────────────────┘
                     │
                     ▼
┌─────────────────────────────────────────┐
│  a cyclonic height anomaly being located  │
│    to the northwestern coast of Australia │
└─────────────────────────────────────────┘
                     │
                     ▼
┌─────────────────────────────────────────┐
│  enhanced cyclonic vorticity, ascending   │
│   motions and water vapor flux convergence│
│   in the northwestern coast of Australia  │
└─────────────────────────────────────────┘
                     │
                     ▼
┌─────────────────────────────────────────┐
│  increased TC geneses and passages in the │
│  northwestern coast of Australia due to   │
│  enhanced relative humidity and cyclonic  │
│  vorticity in the troposphere as favorable│
│   environmental condition for TC genesis  │
└─────────────────────────────────────────┘
```

Figure 12. Schematic of the processes of how the AAO links the TC activity in the southern Indian Ocean during the period of December–March.

analyzed. The averaged height over the northwestern coast of Australia was detrended, and the ENSO years were removed from the newly constructed time series. The ENSO years were determined using the method described in section 2. After these steps, the extreme years were selected as those with absolute values above one standard deviation, and a composite between the extreme years for the height was computed (low-height years minus high-height years) (Figure 11b). The feature of the composite result derived by the simulation is similar to that obtained from observations, i.e., negative anomalies were found over the polar region and the region over the northwestern coast of Australia, and positive anomalies were located in the middle latitudes. These anomalies are significant at the 90% confidence level. The distribution of the height anomalies in the midlatitudes and high latitudes resembles the typical positive AAO phase. Compared with the observation results, the positive height anomalies in the simulation appear to shrink, particularly over the Pacific and Atlantic Oceans. However, the negative height anomaly over the northwestern coast of Australia exhibits a broader area that nearly covers the eastern part of the SIO. Through the analysis above, it can be concluded that the relationship between a positive AAO phase and the negative height anomaly over the northwestern coast of Australia is well captured in the simulation. In general, the similarity between the observation and the simulation results provides additional support for the physical robustness of the AAO-atmospheric circulation links and thus supports the AAO-RH links.

7. Conclusions

[44] In summary, this study examined the linkage between the AAO and the TC activity in the SIO from December to March. During the 1979/1980 to 2010/2011 period, the AAO index has a rank correlation of 0.37 with the TCF in the SIO and is thus significant at the 95% confidence level. Additionally, the ENSO shows a high correlation with the TCF with a rank correlation of -0.33, which is significant at the 93% confidence level. The comparison of the rank partial correlation of the AAO and the ENSO with the TCF revealed that their linkages to the TCF in the SIO are comparable. When the ENSO (AAO) signal is maintained constant, the rank partial correlation between the AAO (ENSO) and the TCF is 0.22 (-0.15). These findings suggest that although the impact of the ENSO on the TCF in the SIO is not negligible, the influence of the AAO on the TCF in the SIO may be noteworthy.

[45] During high-AAO years, TC genesis increases in the northwestern coast of Australia (100°E–120°E and 10°S–30°S). In some grid boxes with a latitude-longitude size of $5° \times 5°$, the amount of the increase in the TC genesis corresponds to 100% compared to the climatology. The TCF in the northwestern coast of Australia has a tight correlation with the AAO index during the DJFM period. The rank correlation is 0.49, which is significant at the 99% confidence level. The increased TC geneses in these regions are accompanied by more frequent TC passages in that region.

[46] The analysis of the GP index demonstrated that when the AAO is in a positive phase, an increase in the RH at the 600 hPa level is thought to be responsible for providing favorable water vapor conditions for TC genesis over the northwestern coast of the Australia, where the TCGF and the TCPF increase. This AAO-RH links may be caused by the weakening of the climatological anticyclone over Australia. When the AAO is in a positive phase, the climatological anticyclone over Australia becomes weak and moves eastward, and a cyclonic circulation anomaly develops over the northwestern coast of Australia. This cyclonic circulation anomaly is not only prone to the formation of ascending motion but also beneficial to the southerly winds located east of the climatological anticyclone in the SIO moving northward to the equator. These enhanced southerly winds transport a high amount of water vapor to the northwestern coast of Australia, which results in the high RH in this region. The relationship between a positive AAO phase and the negative height anomaly over the northwestern coast of Australia, as revealed by the observations described in this study, was also demonstrated through simulations, the results of which support the physical robustness of the AAO-atmospheric circulation links. All of these processes are summarized in Figure 12.

[47] It is worth noting that although changes in humidity in the northwestern coast of Australia are essential to link the AAO and the TC frequency in that region, the relationships between humidity and different types of TCs have not been clarified. For example, a season can be active with a weak/moderate RH, with many tropical storms and a few TC at hurricane intensity, whereas a season can be inactive with a reduced number of TCs but with more than the average concerning the intense cyclones with a high level of RH. Thus, investigation of the linkages between humidity and every stage of TCs is an interesting topic for further work.

[48] Also, it is notable that the AAO-TC links presented in this study exhibit a simultaneous relationship and that the AAO in August has a significant correlation with the DJFM TCF in the SIO. It would be interesting to determine whether there is a linkage between the August AAO on the DJFM

TCF and how this linkage is connected through air-sea processes. Some authors have found that the AAO in boreal autumn is well related to the formation of winter monsoons and that the AAO in boreal winter is related to rainfall during the period of March–May in southern China. The relevant physical mechanisms of these linkages were speculated using the National Center for Atmospheric Research Community Atmospheric Model version 3 (CAM3), and the results indicated that the SST plays an important role through the weakening of the Hadley cell [*Wu et al.*, 2009]. In addition, *Feng et al.* [2010] indicated that there is an apparent inverse relationship between the AAO and the climates in the southwest of Australia. These results imply that the effects of the AAO on climates may not have been stable during recent decades. Thus, we wonder whether the linkage between the AAO and the TC activities in the SIO addressed in this study is stable. These issues require substantial analysis in future works for further clarification of the relationship.

References

Ash, K. D., and C. J. Matyas (2012), The influences of ENSO and the subtropical Indian Ocean dipole on tropical trajectories in the southwestern Indian Ocean, *Int. J. Climatol.*, *32*, 41–56.
Bessafi, M., and M. C. Wheeler (2006), Modulation of south Indian Ocean tropical cyclones by the Madden–Julian oscillation and convectively coupled equatorial waves, *Mon. Weather Rev.*, *134*, 638–656.
Camargo, S. J., K. Emanuel, and A. H. Sobel (2007), Use of a genesis potential index to diagnose ENSO effects on tropical cyclone genesis, *J. Clim.*, *20*, 4,819–4,834.
Camargo, S. J., M. C. Wheeler, and A. H. Sobel (2009), Diagnosis of the MJO modulation of tropical cyclogenesis using an empirical index, *J. Atmos. Sci.*, *66*, 3,061–3,074.
Carton, J. A., G. Chepurin, X. Cao, and B. Giese (2000), A simple ocean data assimilation analysis of the global upper ocean 1950–95, Part I: Methodology, *J. Phys. Oceanogr.*, *30*, 294–309.
Carvalho, L. M. V., C. Jones, and T. Ambrizzi (2005), Opposite phases of the Antarctic oscillation and relationships with intraseasonal to interannual activity in the tropics during the austral summer, *J. Clim.*, *18*, 702–718.
Choi, K.-S., C.-C. Wu, and H.-R. Byun (2012), Possible connection between summer tropical cyclone frequency and spring Arctic Oscillation over East Asia, *Clim. Dyn.*, *38*, 2,613–2,619.
Dee, D. P., et al. (2011), The ERA-Interim reanalysis: Configuration and performance of the data assimilation system, *Q. J. R. Meteorol. Soc.*, *137*, 553–597, doi:10.1002/qj.828.
Emanuel, K. A., and D. S. Nolan (2004), Tropical cyclone activity and global climate, Preprints of the 26th Conference on Hurricanes and Tropical Meteorology, Miami, Fla., pp. 240–241, *Am. Meteor. Soc*, Washington, DC.
Feng, J., J. Li, and Y. Li (2010), Is there a relationship between the SAM and southwest Western Australian winter rainfall?, *J. Clim.*, *23*, 6,082–6,089.
Gent, P. R., et al. (2011), The Community Climate System Model Version 4, *J. Clim.*, *24*, 4,973–4,991, doi:10.1175/2011JCLI4083.1.
Gong, D. Y., and S. Wang (1999), Definition of Antarctic oscillation index, *Geophys. Res. Lett.*, *26*, 459–462.
Gong, D. Y., Y. Gao, D. Guo, R. Mao, J. Yang, M. Hu, and M. Gao (2013), Interannual linkage between Arctic/North Atlantic Oscillation and tropical Indian Ocean precipitation during boreal winter, *Clim. Dyn.*, doi:10.1007/s00382-013-1681-4.
Hall, J. D., A. J. Matthews, and D. J. Karoly (2001), The modulation of tropical cyclone activity in the Australian region by the Madden–Julian oscillation, *Mon. Weather Rev.*, *129*, 2,970–2,982.
Ho, C.-H., J.-H. Kim, H.-S. Kim, C.-H. Sui, and D.-Y. Gong (2005), Possible influence of the Antarctic Oscillation on tropical cyclone activity in the western North Pacific, *J. Geophys. Res.*, *110*, D19104, doi:10.1029/2005JD005766.
Ho, C.-H., J.-H. Kim, J.-H. Jeong, H.-S. Kim, and D. Chen (2006), Variation of tropical cyclone activity in the South Indian Ocean: El Niño–Southern Oscillation and Madden–Julian Oscillation effects, *J. Geophys. Res.*, *111*, D22101, doi:10.1029/2006JD007289.
Knaff, J., and C. R. Sampson (2009), Southern hemisphere tropical cyclone intensity forecast methods used at the Joint Typhoon Warning Center, Part II: Statistical-dynamical forecasts, *Aust. Meteorol. Oceanogr. J.*, *58*, 9–18.
Kuleshov, Y., F. C. Ming, L. Qi, I. Chouaibou, C. Hoareau, and F. Roux (2009), Tropical cyclone genesis in the Southern Hemisphere and its relationship with the ENSO, *Ann. Geophys.*, *27*, 2,523–2,538.
Liebmann, B., and C. A. Smith (1996), Description of a complete (Interpolated) outgoing longwave radiation dataset, *Bull. Amer. Meteor. Soc.*, *77*, 1275–1277.
Marshall, G. J. (2003), Trends in the Southern Annular Mode from observations and reanalyses, *J. Clim.*, *16*, 4,134–4,143.
Nan, S. L., and J. P. Li (2003), The relationship between summer precipitation in the Yangtze River valley and the previous Southern Hemisphere Annular Mode, *Geophys. Res. Lett.*, *30*(24), 2266, doi:10.1029/2003GL018381.
Pohl, B., N. Fauchereau, C. J. C. Reason, and M. Rouault (2009), Relationships between the Antarctic Oscillation, the Madden–Julian Oscillation, and ENSO, and consequences for rainfall analysis, *J. Clim.*, *23*, 238–254.
Ramsay, H. A., S. J. Camargo, and D. Kim (2012), Cluster analysis of tropical cyclone tracks in the Southern Hemisphere, *Clim. Dyn.*, *39*, 897–917.
Saji, N. H., B. N. Goswami, P. N. Vinayachandran, and T. Yamagata (1999), A dipole mode in the tropical Indian Ocean, *Nature*, *401*, 360–363.
Schott, F. A., S.-P. Xie, and J. P. McCreary Jr., (2009), Indian Ocean circulation and climate variability, *Rev. Geophys.*, *47*, RG1002, doi:10.1029/2007RG000245.
Thompson, D. W. J., and J. M. Wallace (2000), Annular modes in the extratropical circulation, Part I: Month-to-month variability, *J. Clim.*, *13*, 1,000–1,016.
Werner, A., A. M. Maharaj, and N. J. Holbrook (2012), A new method for extracting the ENSO-independent Indian Ocean Dipole: Application to Australian region tropical cyclone counts, *Clim. Dyn.*, *38*, 2,503–2,511.
Wilks, D. S. (2006), *Statistical Methods in the Atmospheric Sciences*, 2nd ed., 55–57 pp., Academic Press, Oxford, UK.
Wu, Z., J. Li, B. Wang, and X. Liu (2009), Can the Southern Hemisphere annular mode affect China winter monsoon?, *J. Geophys. Res.*, *114*, D11107, doi:10.1029/2008JD011501.
Zhang, Z. (2010), Reconstruction of Antarctic Oscillation index during past 500 years, PhD thesis, College of Resources and Technology, Beijing Normal Univ., Beijing, China.
Zhou, T. J., and R. C. Yu (2005), Atmospheric water vapor transport associated with typical anomalous summer rainfall patterns in China, *J. Geophys. Res.*, *110*, D08104, doi:10.1029/2004JD005413.
Zhu, Y., and H. Wang (2010), The Arctic and Antarctic oscillations in the IPCC AR4 coupled models, *Acta Meteorol. Sin.*, *24*(2), 176–188.